Variations of LEED intensities with angle of incidence and the influence on spot profiles

G. Held, A. Wander, and D. A. King
University of Cambridge, Department of Chemistry, Lensfield Road, Cambridge CB2 1EW, United Kingdom
(Received 24 January 1995)

We have performed a systematic theoretical study of the effects of variations in the direction of the incoming electron beam on low-energy electron-diffraction (LEED) intensities for the surfaces Ni{111} and $p(2\times2)C$-Ni{111}. Large intensity modulations are observed for variations of the order of 5° in the polar angle of incidence, and the R factor comparison between theoretical I-V curves rise to 1.0 (i.e., no correlation) after varying the polar angle by about 10°–15°. Such data can be used as an independent set of I-V curves to increase the energy range of LEED analyses. Another benefit of collecting data at off-normal incidence directions is that multiple R-factor minima can be shifted or eliminated by changes of 20°–30° in the polar angle. However, we could not see a clear improvement in the sensitivity towards the lateral positions of surface atoms for polar angles below 40°. We have also studied possible effects on measured spot profiles for data taken by scanning through the incidence direction. Serious differences in the relative satellite intensities of split spots which are equal at constant incident angle and additional broadening and distortions of spot shapes could be found for certain angular scan ranges and energies.

I. INTRODUCTION

Since the early days of low-energy electron-diffraction (LEED) I-V analysis it has been known that the shape of I-V curves depends strongly on the incident angle at which the incoming electron beam hits the surface. Parts of the I-V spectra of certain beams can be significantly changed by variations of less than 0.5° in the angles of incidence (see, e.g., Refs. 1 and 2). This fact is routinely exploited in modern LEED experiments in order to achieve normal incidence on low index surfaces where the high surface symmetry is only reflected in the LEED intensities when the incoming electron beam does not break this symmetry, which in most cases requires normal incidence.

Except for early attempts to overcome the multiple-scattering problem by averaging over I-V spectra taken at different directions of incidence (e.g., Refs. 3 and 4) and very few early structure determinations involving dynamical calculations (e.g., Refs. 5–7), off-normal-incidence data are usually not used for quantitative LEED analyses, despite the fact that they potentially contain additional information that could improve the accuracy and reliability of structure determinations as shown by Schmidt *et al.* in a recent paper.[8] This situation has arisen for two main reasons. First, for most off-normal-incidence directions there is no condition like the aforementioned complete equivalence of certain I-V curves which can be used to check the angle of incidence in a relatively convenient way. Second, the exploitation of symmetry can dramatically improve the speed of the calculations involved in any structure determination by LEED, an advantage which is lost if the symmetry is broken by the incidence conditions. The dramatic increase in available computer power seen in the last decade (which will continue into the future) coupled to dramatic increases in speed associated with recent approximations in LEED theory, and improvements in the design of highly accurate UHV manipulators which are already in use for other surface diffraction techniques such as photoelectron diffraction and surface x-ray crystallography, would in principle allow us to extend the range of data collection for LEED crystallography toward exactly defined off-normal angles of incidence. A question, however, which has not yet been systematically addressed concerns the extent of additional information which can be gained by taking extra sets of data, and to what extent LEED crystallography will be improved by so doing. Although LEED I-V spectra contain more relevant information than just the peak positions and heights, it is commonly accepted that the total number of peaks in the available beam spectra—and therefore the total-energy range of the experiment (i.e., the sum of the energy ranges of all spectra)—is a measure of the information retrievable with the current state of theory and data acquisition.[9] There is indeed a great demand for *additional* surface structural information concerning relatively complex systems, such as those involving large adsorbed molecules with many geometrical parameters to be determined. Since recent work has shown that such additional information cannot be expected from the I-V curves of additional beams arising from superstructures with unit cells larger than (4×4) because they are not independent anymore,[10] and since the energy range cannot be extended by much without losing surface sensitivity, the only experimental parameter left to be varied is the incidence direction. In Sec. III of the present work an attempt is made to answer these questions by studying the effects of variations in the angles of incidence for Ni{111} using state of the art LEED theory. Although Ni{111} is a relatively simple surface, we expect the main effects also to be seen for more complex systems.

The considerable intensity variations which we have found even for small changes of incidence angle led us to investigate possible effects on measured profiles of LEED spots which could occur if k space is scanned by varia-

tions of the incidence direction, as is done in some experimental arrangements [e.g., shielded-approximation potential (SPA)-LEED (Ref. 11)]. Quite significant distortions of the true profiles can be found for certain combinations of energy and angles of incidence, which are described in Sec. IV.

II. CALCULATIONS

We have calculated LEED $I(E,\theta_{in},\phi_{in})$ spectra of clean Ni{111} and a $p(2\times2)$ carbon superstructure on the same surface for polar angles between $\theta_{in}=0°$ and 20° (steps of 1°), azimuthal angles between $\phi_{in}=0°$ and 180° (steps of 5°), and energies between 50 and 250 eV (steps of 2 eV). The computer programs were based on the Van Hove/Tong package[12] using standard procedures such as renormalized forward scattering for the stacking of atomic layers and the combined-space method for the evaluation of scattering matrices for layers with more than one atom in the surface unit cell. No use of any symmetry was made, even in those cases where the direction of the incoming electron was within a mirror plane. Therefore, 55 beams for the (1×1) and 177 for the $p(2\times2)$C structure had to be included in the calculations. The atomic-scattering potential for the Ni atoms was taken from the tables by Moruzzi, Janak, and Williams,[13] the phase shifts for carbon were taken from Ref. 12. The parallel components of the incoming wave vector are defined by the angles of incidence as follows:

$$k_{in,x}=|\mathbf{k}_{in}|\sin\theta_{in}\cos\phi_{in}\ ,$$

$$k_{in,y}=|\mathbf{k}_{in}|\sin\theta_{in}\sin\phi_{in}\ ,$$

(the Van Hove/Tong programs use a left-handed coordinate system with the z axis pointing toward the bulk).

For all calculations the coordinate system shown in Fig. 1(a) was used with Ni atoms at (0,0), $\mathbf{a}_1=[\frac{1}{2}a,-(\sqrt{3}/2)a]$ and $\mathbf{a}_2=[\frac{1}{2}a,(\sqrt{3}/2)a]$ ($a=2.49$ Å). With this definition of the basic vectors in real space, the first integral beam appearing along $\phi=-30°$ is labeled (1,0) and that along $\phi=30°$, (0,1) [see Fig. 1(b)]. If not specified otherwise, the nickel substrate was assumed to be bulk terminated (vertical distance between the first and second Ni layers $d_{12}=2.03$ Å), and the carbon atoms were put in fcc hollow sites at a vertical distance of 1.2 Å above the topmost Ni layer. Consequently, even within the superstructure the three mirror planes of the clean unreconstructed surface are maintained along the azimuthal angles of 90°/−90°, 150°/−30°, and 210°/30°, respectively, with the first integral-order LEED beams lying within these mirror planes [see Fig. 1(b)]. The missing half of the full azimuthal range of angles of incidence for any beam can then be obtained by adding the mirrored $I(\theta_{in},\phi_{in})$ spectrum of the beam related to it by the mirror plane along $\phi_{in}=90°/-90°$ to that already calculated.

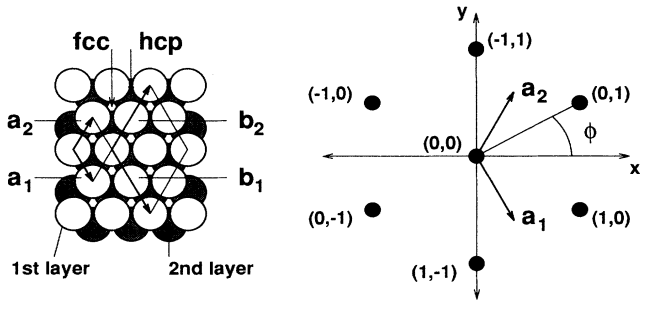

FIG. 1. Coordinate system and surface geometry used in the calculations. The left side (a) shows the real-space arrangement of atoms, threefold adsorption sites, and unit-cell vectors [$a_{1/2}$ for (1×1) and $b_{1/2}$ for (2×2)]; the right side (b) shows the relative orientations of coordinate system, lattice vectors, and LEED beams (i.e., reciprocal-lattice vectors).

The restriction to a comparatively small range of polar incidence angles $\theta_{in}\leq20°$ (in some cases $\leq40°$) was made because diffraction at the surface potential step is ignored in the Van Hove/Tong program package. This is only justified for large enough vertical components of the incident wave vector, i.e., not too large θ_{in}.

III. EFFECTS ON LEED I-V CURVES

A. Results

Examples of $I(\theta_{in},\phi_{in})$ spectra—similar to the isointensity maps proposed in Ref. 6—for the first fractional-order beams of the $p(2\times2)$ superstructure $(-\frac{1}{2},\frac{1}{2})$ and $(\frac{1}{2},-\frac{1}{2})$ and the zeroth and first integral order beams (0,0), (−1,1), and (1,−1) are shown as two-dimensional grey scale plots in Fig. 2 for selected energies.

As expected from the threefold rotational symmetry of the surface, the $I(\theta_{in},\phi_{in})$ spectra of beams related by this symmetry [e.g., (−1,1) and (1,0)] are equal when rotated about 120°. The only symmetry present in the $I(\theta_{in},\phi_{in})$ spectra themselves, however, is with respect to the mirror planes intersecting the respective beams, if there are any. The sixfold symmetry seen in the spectrum of the (0,0) beam, on the other hand, is due to the time-reversal symmetry which relates two opposite incidence directions of this particular beam, and the fact that it is intersected by all three mirror planes.[14,5]

Apparently, the beam intensities can vary quite dramatically even for rather small variations in the angles of incidence—especially θ_{in}—in the order of 5°. This effect is not limited to certain energies, but can be seen over the full energy range under consideration. The shapes of the I-V curves vary accordingly with the angle of incidence, as can be seen from Fig. 3, where the variation of the I-V curves with θ_{in} is shown for the (−1,1) beam of the clean surface at $\phi_{in}=90°$. Calculating the R factors R_P (Ref. 15) and R_{B1} (Ref. 16) between the theoretical curves for the clean surface with $(\theta_{in}=0°,\phi_{in})$ and those with (θ_{in},ϕ_{in}) in order to quantify the changes, shows a more or less linear increase in the R-factor values with θ_{in} up to about 10° for the two tested polar angles $\phi_{in}=60°$ and 90°; this is shown in Fig. 4(a). The R factors reach a value of 1, indicating the complete loss of correlation between the two sets of curves, at angles between 12° and 15°. A similar behavior has also been found for other tested polar angles. However, if I-V curves of individual

beams are compared, the variation of their R factor versus θ_{in} appears to depend more strongly on ϕ_{in}. The steepest increase is found for the azimuthal angles along which the beams under consideration appear [90° for $(-1,1)$, $-90°$ for $(1,-1)$ cf. Fig. 4(b)], reaching R-factor values as large as 2 (indicating anticorrelation), and less steep for the opposite angles.

Naturally, R-factor vs ϕ_{in} plots depend on θ_{in}, since the difference in the parallel component of the incoming k vector increases faster for larger θ_{in}. It is therefore not surprising that the R factor increases faster for larger polar angles of incidence when the azimuth is varied. This can be seen in Fig. 5, where I-V curves (clean surface) of (θ_{in},ϕ_{in}) are compared with those of $(\theta_{in},\phi_{in}=-90°)$ $(\theta_{in}=10°, 20°, \text{and } 30°)$ for the same geometry as before (Fig. 4). For $\theta_{in}=10°$, the R factor reaches 1 only after an

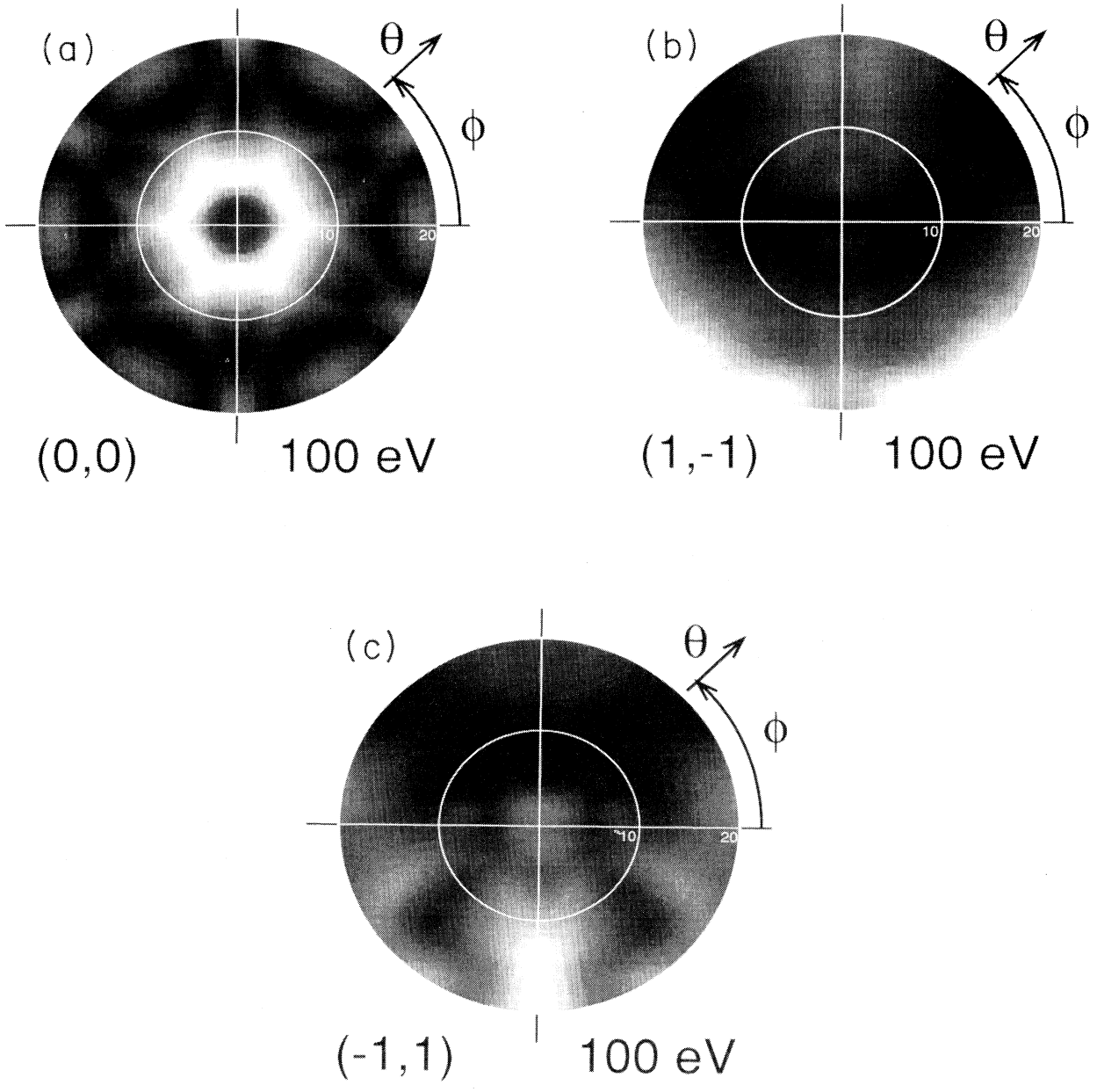

FIG. 2. $I(\theta_{in},\phi_{in})$ grey scale plots for the clean Ni{111} surface: (a) (0,0) at 100 eV, (b) $(1,-1)$ at 100 eV, and (c) $(-1,1)$ at 100 eV; and for the $p(2\times2)$C superstructure: (d) $(\frac{1}{2},-\frac{1}{2})$ at 60 eV and (e) $(-\frac{1}{2},\frac{1}{2})$ at 60 eV. The range of polar angles is from 0° to 20°; the grey scale spans between zero (black) and the maximum intensity value within the given spectrum (white).

azimuthal rotation of 90° while the curves of $\theta_{in}=20°/30°$ reach this value already after about 35°. The dip around $\phi_{in}=30°$ visible in all three curves of Fig. 5 is due to the symmetry of the surface which causes two of the six beams of the first integral order at $\phi_{in}=30°$ and $\phi_{in}=-90°$ to be equivalent.

On the one hand, these effects clearly demonstrate the important of multiple scattering within the surface, since a kinematic theory would only predict minor shifts of the peak positions within the I-V curves and intensity variations on a much larger angular scale, but not such dramatic variations of the peak heights as we have observed. The real questions are, however, how much information could be gained in a LEED intensity analysis if data were also taken at off-normal incidence, and what would be a reasonable (θ_{in},ϕ_{in}) grid on which to take data. In order to address these questions we have calculated R factors between theoretical I-V curves for different angles of incidence and different geometries which were given by the variation of single parameters. The parameters chosen were the distance between the first and second Ni layer d_{12} in the (1×1) structure and a symmetric lateral shift Δs of Ni atoms in the first layer in the $p(2\times2)$ structure. They represent two problems which occur frequently in LEED analyses, namely the existence of multiple R-factor minima about 0.5 Å apart when vertical parameters are varied, and the relative insensitivity toward geometrical parameters parallel to the surface.

R_P vs d_{12}

LEED intensity spectra were calculated for Ni{111} with a first interlayer spacing of 2.03 Å, and these were used as reference spectra for a simulated analysis. Figure 6(a) shows R_P vs d_{12} plots at $\phi_{in}=\pm90°$ (i.e., along a mirror plane) and four different polar angles $\theta_{in}=0°$, 10°, 20°, and 30° in which I-V curves of the first integral-order beams were calculated for trial geometries with d_{12} between 1.90 and 3.20 Å (steps of 0.025 Å). Except for the true global minimum, two other distinct minima can clearly be seen at polar angles $\theta_{in}=0°$, 10°, and 20° in the given geometry range at d_{12} value between 2.5 and 2.6 Å and also between 2.85 and 2.95 Å. These spurious minima could be expected to have similar depth to that of the true minimum when the comparison is done with experimental data instead of calculated I-V curves. At $\theta_{in}=30°$, however, only one very broad additional minimum appears in each plot, around 2.65 Å for $\phi_{in}=+90°$ and between 2.8 and 2.9 Å for $\phi_{in}=-90°$. More importantly, if the plots for ±90° are averaged, there are no more distinct minima left in the regime between 2.6 and 3.0 Å. For the same polar angles and the two opposite azimuths, $\phi_{in}=60°$ and $-120°$, pronounced R-factor minima in addition to the true minimum exist only for $\theta_{in}=0°$ and 10° [Fig. 6(b)]. For the two other polar angles, the regime above 2.55 Å is rather a broad regime of lower R factors, and not a genuine minimum. It is remarkable that in this latter case the R_P vs d_{12} curves of the two opposite azimuthal angles, which are not parallel to a mirror plane of the surface, are almost identical, which is not the case of $\phi_{in}=\pm90°$ (parallel to a mirror plane).

Lateral shifts

In a second approach to test the influence of variations of the angles of incidence on the reliability of I-V analy-

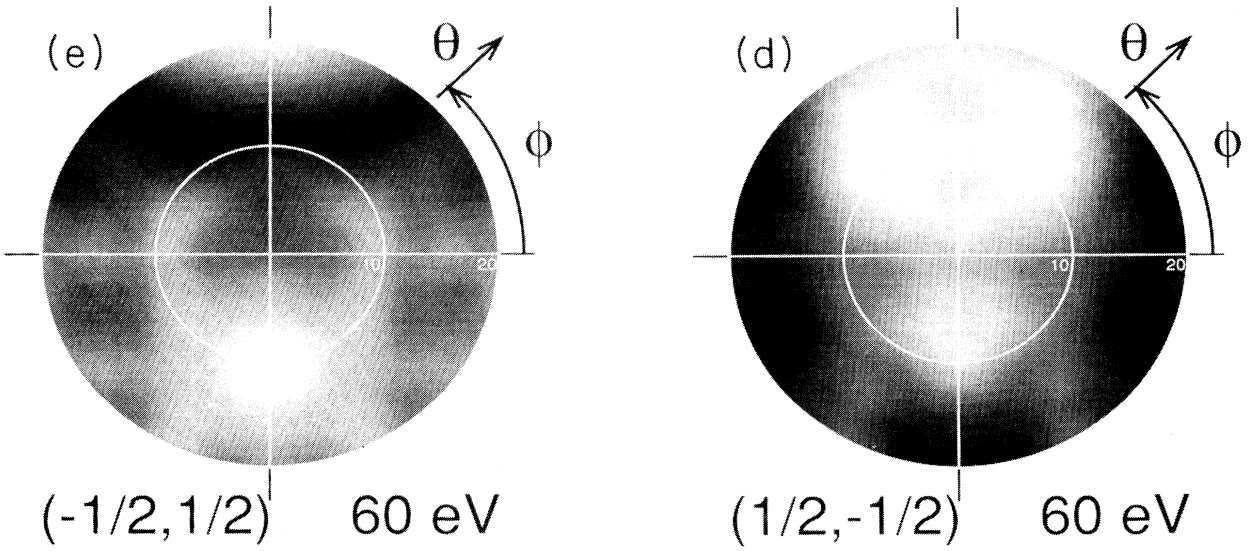

FIG. 2. (*Continued*).

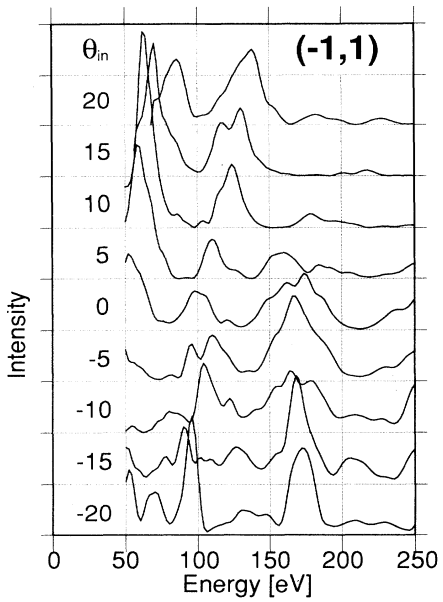

FIG. 3. I-V curves of the $(-1,1)$ beam for different polar angles of incidence $-20° \leq \theta_{in} \leq 20°$ at $\phi_{in} = \pm 90°$ (negative polar angles correspond to $\phi_{in} = -90°$).

ses, we compared the R factors of $p(2\times2)$-C structures with different lateral displacements of substrate atoms in the topmost layer. Only the atoms surrounding the fcc sites with C atoms adsorbed in them were displaced along the mirror planes in order to preserve the overall C_{3v} symmetry of the surface and to avoid the necessity of domain mixing which would otherwise arise. The vertical layer distances were kept at 1.20 Å between adsorbate and substrate and 2.03 Å between first and second Ni layers. The R factors between the I-V curves (the first integral order and first two fractional orders) for three nonzero shifts Δs (0.05, 0.10, and 0.20 Å) and those of the undisturbed first layer are listed in Table I for $\phi_{in} = 90°$ (parallel to one of the displacement vectors) and 60° and polar angles between 0° and 40°. Surprisingly, we find the largest R_P sensitivity toward small lateral displacements (0.05 and 0.10 Å) for $\theta_{in} = 0°$, which is evident from the larger R-factor values at this angle. Only for the very large displacements of 0.20 Å is R_P higher for most (but not all) off-normal angles of incidence.

Another equally important finding is that the two R factors R_P and R_{B1} disagree in their minimum values, while the minima found in other LEED I-V analyses performed with both R factors usually agree very well (e.g., Ref. 16). We therefore reach the somewhat disappointing conclusion that there is not a clear tendency toward more sensitivity for lateral displacements at higher off-normal angles of incidence even up to 40° from the surface normal.

B. Discussion: Implications for I-V analyses

The motivation for the present work was to explore the possible benefits of taking data at off-normal angles of incidence for structure determinations by LEED. Although we have studied only one surface, Ni{111}, we assume that our findings reflect general tendencies which apply similarly to other surfaces. Two of the results found in Sec. III A are very promising.

(i) Two sets of I-V curves are completely uncorrelated (i.e., $R_P = 1$) when they differ in polar angle of incidence by 10°–15°.

(ii) R-factor minima which are not true minima can be shifted or completely eliminated by choosing different incidence directions.

According to the first finding the number of independent I-V curves, and therefore the total-energy range for an I-V analysis, can be increased effectively by taking data not only at $\theta_{in} = 0°$ but also at, e.g., $\theta_{in} = 15°$ and 30°. The R-factor variation with ϕ_{in} at these polar angles is

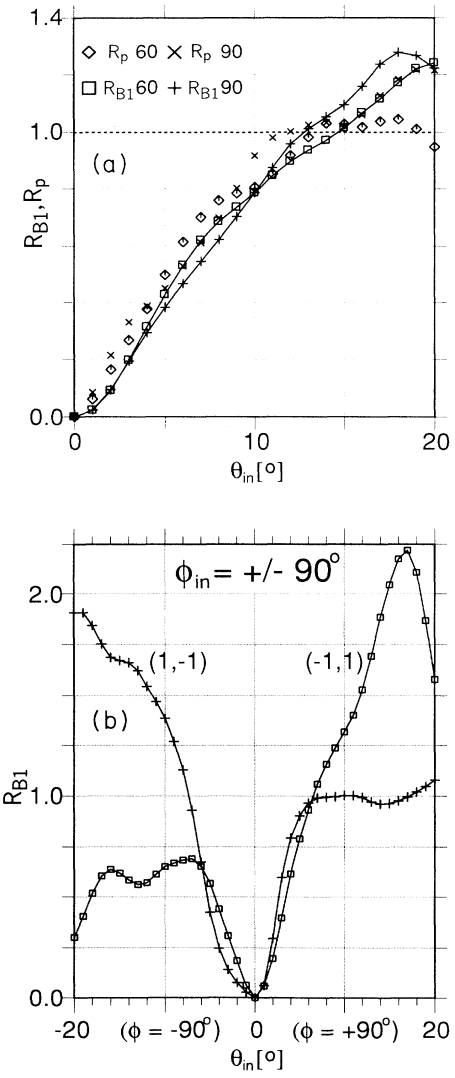

FIG. 4. (a) R factors R_P and R_{B1} vs θ_{in} averaged over the (0,0) beam and the first-order beams of Ni{111} at the two azimuths $\phi_{in} = 60°$ and 90°. (b) R factors R_{B1} vs θ_{in} for the two single beams $(-1,1)$ and $(1,-1)$ at $\phi_{in} = \pm 90°$ (negative polar angles correspond to $\phi_{in} = -90°$). The I-V curves for $\theta_{in} = 0$ are compared with those for the indicated polar angle of incidence.

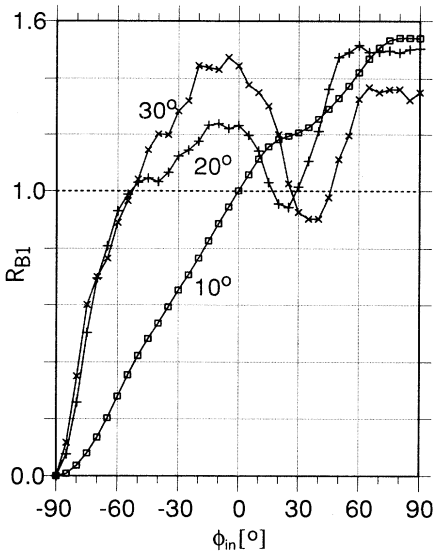

FIG. 5. Averaged R factors R_{B1} vs ϕ_{in} for the (0,0) beam and the first-order beams of Ni{111} at three polar angles of incidence $\theta_{in}=10°$, 20°, and 30°. The I-V curves for $\phi_{in}=90°$ are compared with those for the indicated azimuthal angle of incidence.

smaller because the variation of ϕ_{in} does not imply that much change in the incident k vector, and also the symmetry of the particular surface has to be considered. Nevertheless, at least two independent sets of data should be measurable at each polar angle. Due to the high symmetry of the LEED pattern at normal incidence, the amount of normal-incidence data is additionally reduced as beams of each order of Ni{111} are at least threefold degenerate. Four additional sets of data (two azimuths at the two polar angles) would therefore lead to at least a 13-fold ($4\times3+1$) increase in the energy range available for comparison with calculated I-V curves. Such an increase in the energy range would lower Pendry's RR factor, the relative uncertainty at the R-factor minimum,[15] as follows:

$$\frac{RR_{\text{offn}}}{RR_{\text{norm}}}=\sqrt{\tfrac{1}{13}}=0.28\ . \tag{1}$$

Conventionally, the error bar for a particular geometrical parameter p is determined as the parameter range which leads to R factors between $R_{\min}$ and $(1+RR)R_{\min}$. Assuming a quadratic dependence of the R factor on variation of the parameter p in the vicinity of the minimum such as

$$R(\delta p)=R_{\min}+\alpha(\delta p)^2\ , \tag{2}$$

the reduction in the error bar Δp can then be calculated as

$$\frac{(\Delta p)_{\text{offn}}}{(\Delta p)_{\text{norm}}}=\left[\frac{RR_{\text{offn}}}{RR_{\text{norm}}}\right]^{1/2}=(\tfrac{1}{13})^{1/4}=0.52 \tag{3}$$

(we tacitly assume that α and $R_{\min}$ remain unchanged when off-normal data are included). Such a factor 0.5 in the error bar could indeed often make the difference between significant and insignificant distortions of chemical bonds.

Not only can the precision of LEED intensity analyses be improved in this way, but also the structural reliability, when multiple minima are shifted or eliminated through the use of multiple data sets. A similar effect is observed for LEED data taken at normal incidence when additional beams (or a wider energy range) are included in the analysis. Only the true minimum should appear at the same geometrical parameters under all conditions. As can be seen from Figs. 6(a) and 6(b), the change in the polar angle necessary to reach these effects may depend on the azimuthal orientation of the incident beam. A change of 30°, however, was sufficient to alter the shape of the R-factor plots significantly in the regime outside the vicinity of the true minimum for all four azimuths

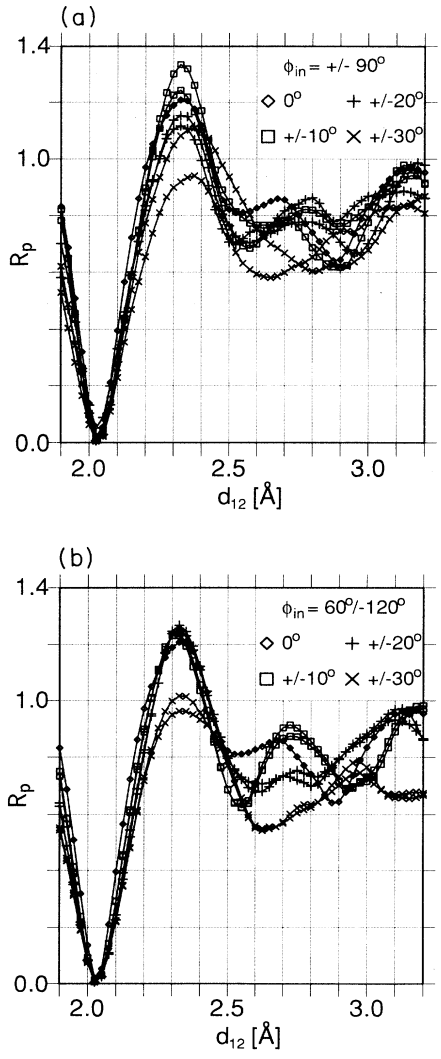

FIG. 6. Averaged R factor R_P (same beams as in Fig. 5) vs d_{12} for different polar and azimuthal angles of incidence: (a) $\phi_{in}=90/-90°$; $\theta_{in}=0°(\diamond)$, 10°(□), 20°(+), and 30°(×). (b) $\phi_{in}=60/-120°$; $\theta_{in}=0°(\diamond)$, 10°(□), 20°(+), and 30°(×).

TABLE I. R factors between sets of I-V curves calculated for lateral shifts Δs of substrate atoms and those of an undistorted substrate; see text for details.

	Δs	0.00 Å vs 0.05 Å		0.00 Å vs 0.10 Å		0.00 Å vs 0.20 Å	
θ_{in}	ϕ_{in}	R_P	R_{B1}	R_P	R_{B1}	R_P	R_{B1}
0°		0.1650	0.0243	0.3386	0.0984	0.4517	0.2797
10°	90°	0.1188	0.0367	0.2788	0.1203	0.4967	0.2433
	75°	0.1317	0.0343	0.3153	0.1168	0.5138	0.2448
	60°	0.1142	0.0404	0.2745	0.1367	0.4967	0.3058
20°	90°	0.0934	0.0209	0.2273	0.0667	0.4877	0.1894
	75°	0.0949	0.0195	0.2253	0.0661	0.3987	0.2215
	60°	0.0872	0.0342	0.2411	0.1171	0.4670	0.3038
30°	90°	0.0831	0.0242	0.2046	0.1020	0.4109	0.3142
	75°	0.1084	0.0364	0.2496	0.1185	0.4440	0.2415
	60°	0.1098	0.0453	0.2874	0.1604	0.5413	0.3553
40°	90°	0.0864	0.0202	0.1846	0.0672	0.3647	0.1645
	75°	0.1084	0.0316	0.2629	0.1044	0.4792	0.2666
	60°	0.1043	0.0506	0.3170	0.1583	0.6044	0.3887

that we have studied. Therefore, an experimental data set including various angles of incidence will provide less traps (i.e., local R-factor minima) for automated refinement procedures of surface structures if the refinement is done simultaneously for all angles; a discrimination between the remaining minima will also be easier because of the expected greater difference in the actual R-factor values and the smaller error bars.

The finding that there is no clearly increased sensitivity for lateral displacements at off-normal incidence directions in the studied angular range up to $\theta_{in}=40°$ is rather disappointing. The large scatter and sometimes diverging tendencies of the two R factors, R_P and R_B, show that the degrees and the kinds of modifications in the I-V curves due to lateral displacements are different for different incidence conditions (R_P is more sensitive to the peak positions while the relative intensities of the peaks are more relevant for R_B). The explanation for this behavior probably lies in the shape of the scattering factor for Ni atoms $|f(\theta_s)_{Ni}|^2$ (see Fig. 7). Within the energy range of our calculations, there are deep minima in $|f(\theta_s)_{Ni}|^2$ for scattering angles θ_s just below 90° (70°–80°). Exactly these angles, however, are decisive for the relevance of intralayer scattering because they provide the transition from the dominant forward-scattering directions into directions parallel to the surface. Since intralayer scattering is to a large extent responsible for the sensitivity of LEED intensities toward lateral displacements inside the surface unit cell, it seems reasonable to assume that this sensitivity decreases when some atoms in the layer appear under the minimum scattering angle (70°–80°) with respect to the incoming beam. The number of such atoms depends, of course, on the particular set of angles of incidence (θ_{in} *and* ϕ_{in}), but there should always be some atoms affected in the polar range between 10° and 40° which we have studied.

The shape of $|f(\theta_s)|^2$ is different for other atoms; therefore this finding cannot be generalized and has to be tested in every particular case. However, on the grounds of the above discussion a dramatic increase in the lateral sensitivity may be expected for incidence directions where a significant portion of the forward-scattering peak propagates parallel to the surface, i.e., $\theta_{in}>70°$. Our findings are therefore not in conflict with the results of Schmidt *et al.*, who have found a significantly increased sensitivity in R_P toward lateral relaxations on W{100} for a polar angle of incidence θ_{in} of around 74°, as compared to normal incidence.[8] We feel, however, that for an accurate structure determination at such slanting incidence angles the influence of the potential step would have to be included more accurately than is currently done in standard LEED codes. At these incidence conditions the normal energy component is comparable to the height of the potential step, and consequently scattering from the surface barrier cannot be neglected; in addition,

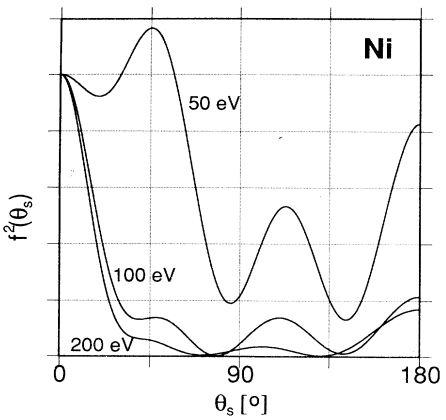

FIG. 7. Atomic-scattering factor $|f(\theta_s)|^2$ for Ni vs scattering angle θ_s for 50, 100, and 200 eV.

a simple step function can then not be expected to model the shape of this barrier sufficiently. In effect, we are dealing with *V*LEED problems at LEED energies.

IV. EFFECTS ON SPOT PROFILES

Some experimental systems used to measure LEED spot profiles scan the k_{out} space by actually varying the angle of incidence [e.g., SPA-LEED (Ref. 11)]. Given the strong intensity variations which we have just described, it was clearly important to investigate the effect on spot profiles recorded in this way. The very assumption on which most conclusions from spot profile analyses rest is that the so-called structure factor $F(\mathbf{k}_{out})$ reflecting the dynamical scattering of electrons within the local environment of the scatterers is practically constant as a function of $\mathbf{k}_{out}$ in the vicinity of a beam at $\mathbf{k}_{out}=\mathbf{k}_g$,[17] so that the recorded LEED intensity profile

$$I(\mathbf{k}_{out})=F(\mathbf{k}_g)\times G(\mathbf{k}_{in}-\mathbf{k}_{out}) \quad (\mathbf{k}_{out}\sim\mathbf{k}_g) \tag{4}$$

is determined only by the lattice factor $G(\mathbf{k}_{in}-\mathbf{k}_{out})$. This latter factor is essentially the Fourier transform of the autocorrelation functions of the scatterers, and therefore contains all information about long-range order on the surface. The slow variation of $F(\mathbf{k}_{out})$ has indeed been shown by a number of theoretical and experimental studies at constant initial state, i.e., a fixed direction of the incoming electron beam (e.g., Refs. 18, 10, and 19). The situation changes, however, if instead the modulus of the momentum transfer $|\mathbf{k}_{in}-\mathbf{k}_{out}|$ is kept constant (as for SPA-LEED) and therefore $\mathbf{k}_{in}$ is varied along with the scan through $\mathbf{k}_{out}$. Since F is obviously a function of both $\mathbf{k}_{in}$ and $\mathbf{k}_{out}$, slowly varying with the latter but rapidly varying with the first, the situation is better described by the following equation:

$$I(\mathbf{k}_{in},\mathbf{k}_{out})=F(\mathbf{k}_{in},\mathbf{k}_g)\times G(\mathbf{k}_{in}-\mathbf{k}_{out}) \quad (\mathbf{k}_{out}\sim\mathbf{k}_g)\ , \tag{5}$$

where G depends only on the momentum transfer $\mathbf{k}_{in}-\mathbf{k}_{out}$ and is therefore independent of the actual angle of incidence. Thus we can calculate the expected spot profiles for a given shape of $G(\mathbf{k}_{in}-\mathbf{k}_{out})$ (the quantity which is actually wanted for a profile analysis) according to this formula with $F(\mathbf{k}_{in},\mathbf{k}_g)\propto I_g(\theta_{in},\phi_{in})$ (the calculated LEED intensity for the spot g).

A. Results

We studied possible change in spot profiles due to angle-of-incidence variations using the above formula for two typical examples for which the gross shape of G is known and easy to calculate: spot splitting of integral-order beams due to a periodic arrangement of steps on the surface, and spot broadening of fractional-order beams due to formation of small islands.

Spot splitting

For a regularly stepped surface, symmetric spot splitting is observed when the out-of-phase condition is fulfilled for the electrons backscattered from two consecutive terraces. According to the formula given by Henzler,[20] this is the case for the (0,0) beam at energies

$$E_{(0,0)}=\left[\frac{s}{\cos\theta_{in}}\right]^2\frac{37.5V\ \text{Å}^2}{d_\perp^2}\ ,$$

where $d_\perp$ is the vertical separation of the terraces in Å, and $s=n+\frac{1}{2}$ a half-integer number. For the interlayer distance of Ni{111}$d_\perp=2.03$ Å and $s=\frac{5}{2}$ the calculated energy is 56.8 eV, if we assume θ_{in} to be small (i.e., $\cos\theta_{in}\sim 1$). For example, with a [6(111)×(100)] surface (terraces which are six close-packed rows wide separated by monoatomic steps along the close-packed rows), the distance in k space between the two satellite spots is one-sixth of the length of a reciprocal-lattice vector. For 56.8 eV and an angle between $\mathbf{k}_{in}$ and $\mathbf{k}_{out}$ close to 180° (within ~30°), this would correspond to a variation of the polar angle of incidence of 3.7° if $|\mathbf{k}_{in}-\mathbf{k}_{out}|$ is kept constant. The main contribution to the dynamical scattering on such a surface is still due to the atoms within the terraces rather than the step atoms, and it therefore seems justified to use the $I(\theta_{in},\phi_{in})$ spectra calculated for the flat {111} surface.

Assuming a large transfer width of the system and a well-ordered stepped surface, the relative intensities of the two satellite spots can be calculated by multiplying δ-like functions of unit weight (i.e., idealized spot profiles) with the intensity of the (0,0) beam at the corresponding angle of incidence. In Fig. 8 this is shown for $\phi_{in}=90°$ and two different angle regimes of θ_{in}, namely with the (0,0) beam centered at 4.6° and at 15.2°, respectively (for constant $|\mathbf{k}_{in}-\mathbf{k}_{out}|$ this corresponds to angles of 171° and 150° between the two vectors).

Despite the symmetric splitting of the spot profile due to the lattice factor G, dramatic differences can be seen in the relative intensities between the two pairs of satellite

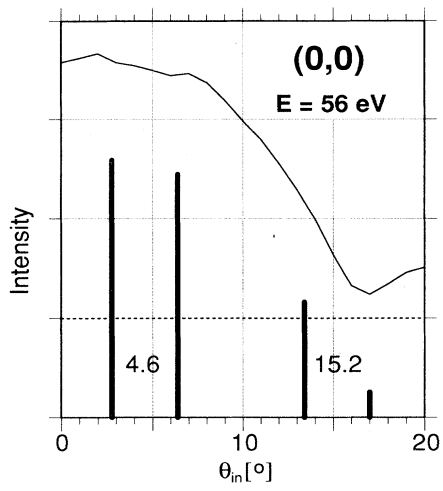

FIG. 8. $I(\theta_{in})$ curve for the (0,0) beam (solid curve, $\phi_{in}=90°$) and intensities of the two satellite spots (rods) at 56 eV for two different scan ranges of the incoming electron beam. The polar angles 4.6° and 15.2° specified in the diagram refer to angle of incidence where the center of the (0,0) beam would hit the detector.

spots. While for 4.6° the intensities are almost identical and therefore resemble the symmetry of G quite well, in the 15.2° case one satellite spot appears about four times more intense than the other. If this initial-state effect is not handled carefully in the second case, it could lead to a misinterpretation of the structural properties of the surface, such as step separations which are either too small or too large.

Spot broadening

Similar angle-of-incidence effects can be expected on the profiles of broad spots with widths not determined by the transfer width of the experimental system but by the finite size of ordered areas on the surface. Obviously, one would expect additional broadening if the center of the spot coincides with a narrow minimum in the $I(\theta_{in},\phi_{in})$ curve and widths which are too small if it does with a sharp peak in $I(\theta_{in},\phi_{in})$. In order to explore these effects more accurately, we assumed a Lorentzian shape of G with a true width of 2° in θ_{in} (FWHM), which at 100 eV corresponds to a linear island size of about ten lattice constants. The LEED beams under consideration were those of the first fractional order of the $p(2\times2)$C-Ni{111} superstructure, namely $(-\frac{1}{2},\frac{1}{2})$ and $(\frac{1}{2},-\frac{1}{2})$ at $\phi_{in}=90°$, with variations only in θ_{in}. Figure 9 shows spot profiles of $(\frac{1}{2},-\frac{1}{2})$ at 98 eV centered at angles θ_{in} between 8° and 12° together with the corresponding $I(\theta_{in})$ curve. For the spot centered at the minimum of the $I(\theta_{in})$ curve at 8°, scanning through the angle of incidence leads to a profile width of 3.1° which decreases toward the true value of 2° and becomes even slightly smaller when the center of the spot is shifted to higher incidence angles (the profile widths are given as parameters in Fig. 9). Consequently, this could lead to errors of more than 30% in the determination of island sizes.

A similar effect can be seen when, instead of the scanning range of the angle of incidence, the energy is changed which again can cause a minimum in the $I(\theta_{in})$ curve to coincide with the center of the spot and therefore additionally broaden the observed profile. Two examples are shown in Fig. 10 for energies between 90 and 98 eV and the $(\frac{1}{2},-\frac{1}{2})$ spot centered at two different θ_{in}, 8° and 12° (since the length of the k vector varies by less than 5% in the given energy range, we assumed the spot to be centered at the same θ_{in} for all energies). Not only are changes in widths of the spot profiles seen, by about the same amount as before, but also the maximum position is slightly shifted for 94 eV at $\theta_{in}=15°$ with respect to 90 and 98 eV.

Finally we investigated the influence of slight structural changes, such as changes in the interlayer spacings, on the spot profiles, again assuming the same shape of G as before. For this purpose, we calculated $I(\theta_{in},\phi_{in}=90°)$ spectra for $p(2\times2)$C-Ni{111} with C-Ni layer distances of 1.0 and 1.1 Å in addition to the 1.2 Å that were already calculated. A most dramatic effect was found for the $(-\frac{1}{2},\frac{1}{2})$ beam at 70 eV around $\theta_{in}=11°$ (see Fig. 11). Due to the almost complete extinction of the beam intensity for a layer distance of 1.1 Å at $\theta_{in}=11°$, the spot profile splits up into two satellites about 4° apart. This is not the case for the layer distances 1.0 and 1.2 Å, for which the main part of the profile is very similar to the shape of G. A spot profile analysis based only on this single set of data would probably postulate a domain-wall structure in the first case and islands without interdomain

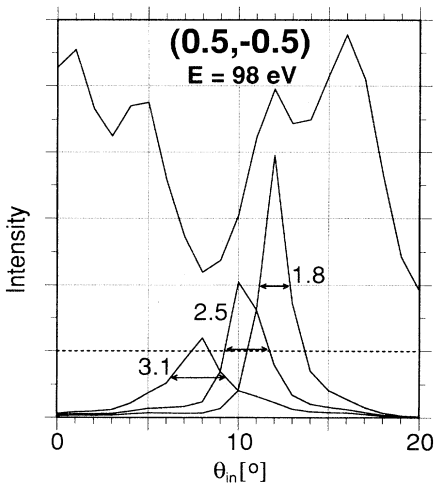

FIG. 9. Changes in spot profiles of the $(\frac{1}{2},-\frac{1}{2})$ beam (98 eV, $\phi_{in}=90°$) upon variations of the polar angle of incidence. The curve on top is the $I(\theta_{in})$ curve of $(\frac{1}{2},-\frac{1}{2})$, the three spot profiles at the bottom are calculated according to Eq. (5) as the product of Lorentzian G functions (the FWHM is 2°) centered at $\theta_{in}=8°$, 10°, and 12° with $I(\theta_{in})$. The parameters given in the figure are the FWHM (in degrees) of the resulting profiles.

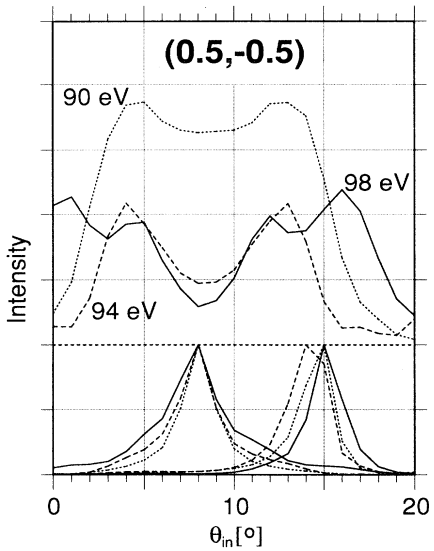

FIG. 10. Changes in spot profiles of the $(\frac{1}{2},-\frac{1}{2})$ beam ($\phi_{in}=90°$) upon variations of energy. The upper part of the figure shows the $I(\theta_{in})$ curves for energies of 90 (dotted), 94 (dashed), and 98 eV (solid); the corresponding spot profiles for Lorentzian G functions (the FWHM is 2°) centered at two different polar angles of incidence (8° and 15°) are shown below. For better comparability, the spot profiles are normalized to the same maximum height.

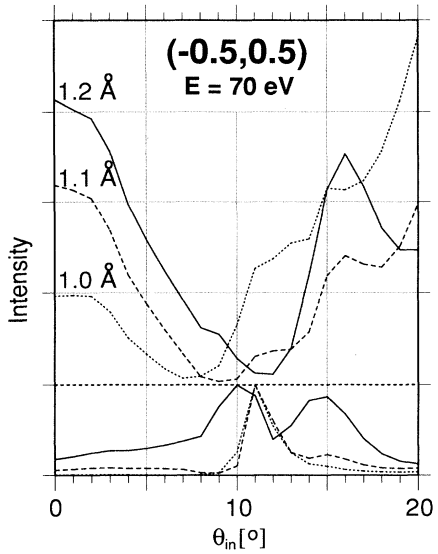

FIG. 11. Changes in spot profiles of the $(-\frac{1}{2},\frac{1}{2})$ beam (70 eV, $\phi_{in}=90°$) upon variations of the adsorbate geometry. The upper part of the figure shows the $I(\theta_{in})$ curves for adsorbate-substrate layer distances of 1.0 (dotted), 1.1 (dashed), and 1.2 Å (solid); the corresponding spot profiles for Lorentzian G functions (the FWHM is 2°) centered at $\theta_{in}=11°$ are shown below. For better comparability, the spot profiles are normalized to the same maximum height.

order in the latter case. Coadsorption, for example, can always lead to such changes in the surface geometry. Therefore conclusions about changes in the island sizes upon coadsorption have to be handled carefully.

In addition to the changes in the spot widths, it should also be noted that all profiles in Figs. 9, 10, and 11 are asymmetric, for which also many examples can be found among the published SPA-LEED data (e.g., Ref. 21). Asymmetric profiles are expected whenever the centers of the spots do not coincide with symmetric extrema of the $I(\theta_{in})$ curves.

B. Discussion

The above examples were deliberately chosen from the worst cases we could find within our theoretical data set to demonstrate that multiple-scattering effects can distort the measured profile of LEED spots significantly if they are recorded by varying the direction of the incoming electron beam (i.e., the initial state). Very strong effects are, however, exceptional, although they can be found all over the ranges of energy and angles of incidence used for spot profile analyses. It is therefore good advice to measure profiles at several different combinations of energy and/or incidence directions in order to eliminate undesired initial-state effects.

V. SUMMARY

We have performed a systematic theoretical study of effects of variations in the direction of the incoming electron beam on LEED intensities for the surfaces Ni{111} and $p(2\times2)$C-Ni{111}. The pertinent results for LEED I-V analyses are as follows.

(i) Two sets of I-V curves are completely uncorrelated (i.e., $R_P=1$) with a difference in the polar incidence angle of 10° to 15°.

(ii) Spurious R-factor minima, in addition to the true minimum, can be shifted or completely eliminated by choosing a different incidence direction.

(iii) For polar angles $\leq 40°$ there is no significantly increased sensitivity for lateral displacements at off-normal angles of incidence.

We conclude that additional data taken at off-normal incidence can improve the precision and reliability of LEED I-V analyses.

We have also studied effects on measured spot profiles where the data are taken by varying the incidence direction. Large differences in the relative intensities of actually equally intense satellites of split spots and additional broadening and distortions of spot shapes can be found for certain angular scan ranges.

ACKNOWLEDGMENT

The EPSRC is acknowledged for postdoctoral support to G.H.

[1]M. K. Debe and D. A. King, J. Phys. C **15**, 2257 (1982).
[2]G. Michalk, W. Moritz, H. Pfnür, and D. Menzel, Surf. Sci. **129**, 92 (1983).
[3]T. C. Ngoc, M. G. Lagally, and M. B. Webb, Surf. Sci. **35**, 177 (1973).
[4]D. Aberdam, R. Baudoing, C. Gaubert, and E. G. McRae, Surf. Sci. **57**, 715 (1976).
[5]B. W. Holland, R. W. Hannum, A. M. Gibbons, and D. P. Woodruff, Surf. Sci. **25**, 576 (1971).
[6]Groupe d'Études des Surfaces, Surf. Sci. **48**, 496/509 (1975); **62**, 567 (1977).
[7]E. Zanazzi, F. Jona, D. W. Jepsen, and P. M. Marcus, Phys. Rev. B **14**, 432 (1976).
[8]G. Schmidt, H. Zagel, H. Landskron, K. Heinz, K. Müller, and J. B. Pendry, Surf. Sci. **271**, 416 (1992).
[9]M. A. Van Hove, W. H. Weinberg, and C. M. Chan, *Low-Energy Electron Diffraction,* Springer Series in Surface Science Vol. 6 (Springer-Verlag, Berlin, 1986).
[10]K. Heinz, U. Starke, M. A. Van Hove, and G. A. Somorjai, Surf. Sci. **261**, 57 (1992).
[11]U. Scheithauer, G. Meyer, and M. Henzler, Surf. Sci. **178**, 441 (1986).
[12]M. A. Van Hove and S. Y. Tong, *Surface Crystallography by LEED* (Springer-Verlag, Berlin, 1979).
[13]V. L. Moruzzi, J. F. Janak, and A. R. Williams, *Calculated Electronic Properties of Metals* (Pergamon, New York, 1978).
[14]D. P. Woodruff and B. W. Holland, Phys. Lett. **31A**, 207 (1970).
[15]J. B. Pendry, J. Phys C **13**, 937 (1980).
[16]G. Held, H. Pfnür, and D. Menzel, Surf. Sci. **271**, 21 (1992).

[17]M. Henzler, Surf. Sci. **152/153**, 963 (1985).
[18]H. Jagodzinski, W. Moritz, and D. Wolf, Surf. Sci. **77**, 223 (1978); **77**, 249 (1978); **77**, 265 (1978); **77**, 283 (1978).
[19]K. Heinz, U. Starke, and F. Bothe, Surf. Sci. Lett. **243**, L70 (1991).
[20]M. Henzler, in *Electron Spectroscopy for Surface Analysis,* edited by H. Ibach (Springer-Verlag, Berlin, 1977), p. 117.
[21]M. Sokolowski and H. Pfnür, Phys. Rev. B **49**, 7716 (1994).

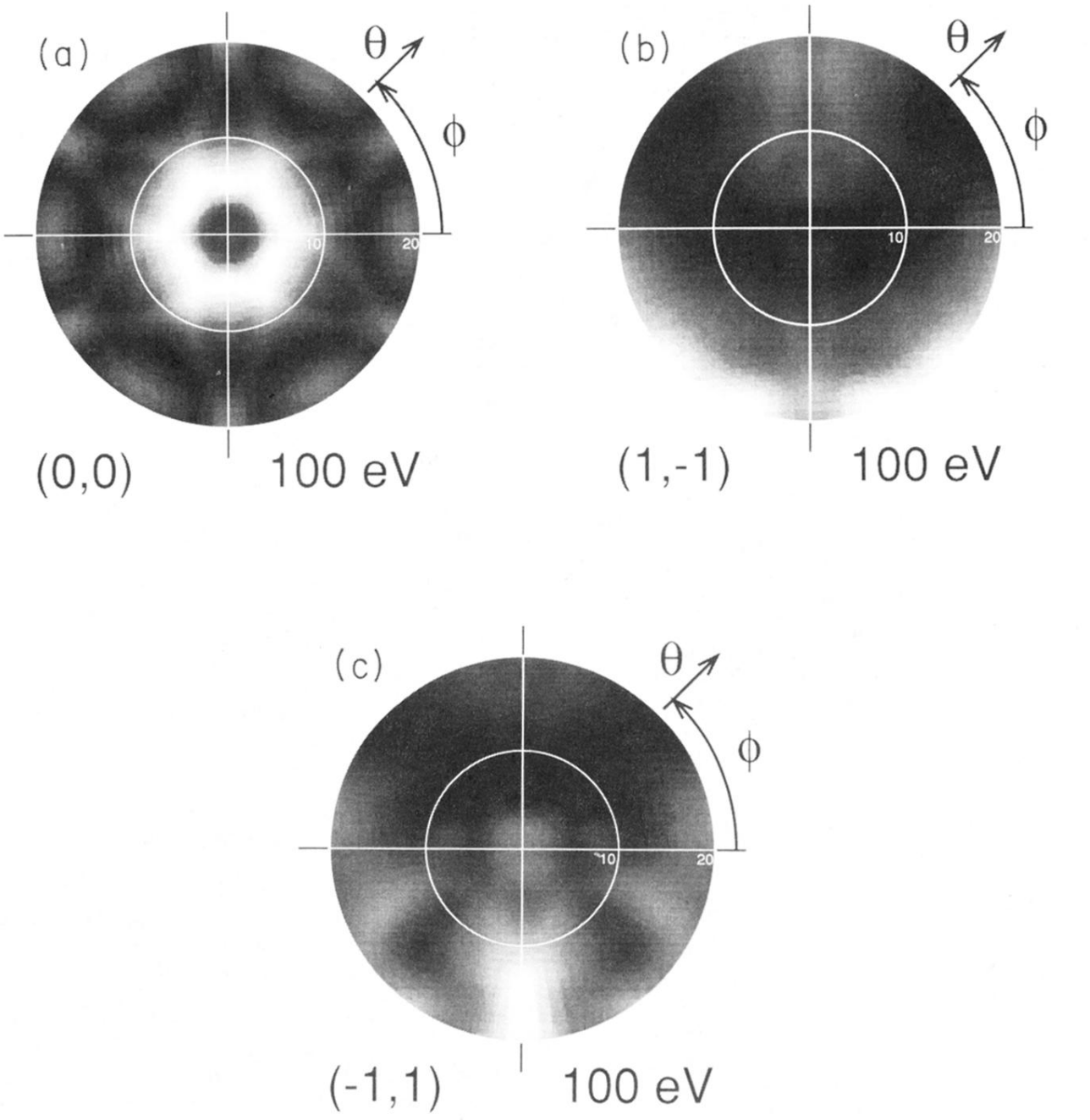

FIG. 2. $I(\theta_{in},\phi_{in})$ grey scale plots for the clean Ni{111} surface: (a) (0,0) at 100 eV, (b) $(1,-1)$ at 100 eV, and (c) $(-1,1)$ at 100 eV; and for the $p(2\times2)$C superstructure: (d) $(\frac{1}{2},-\frac{1}{2})$ at 60 eV and (e) $(-\frac{1}{2},\frac{1}{2})$ at 60 eV. The range of polar angles is from 0° to 20°; the grey scale spans between zero (black) and the maximum intensity value within the given spectrum (white).

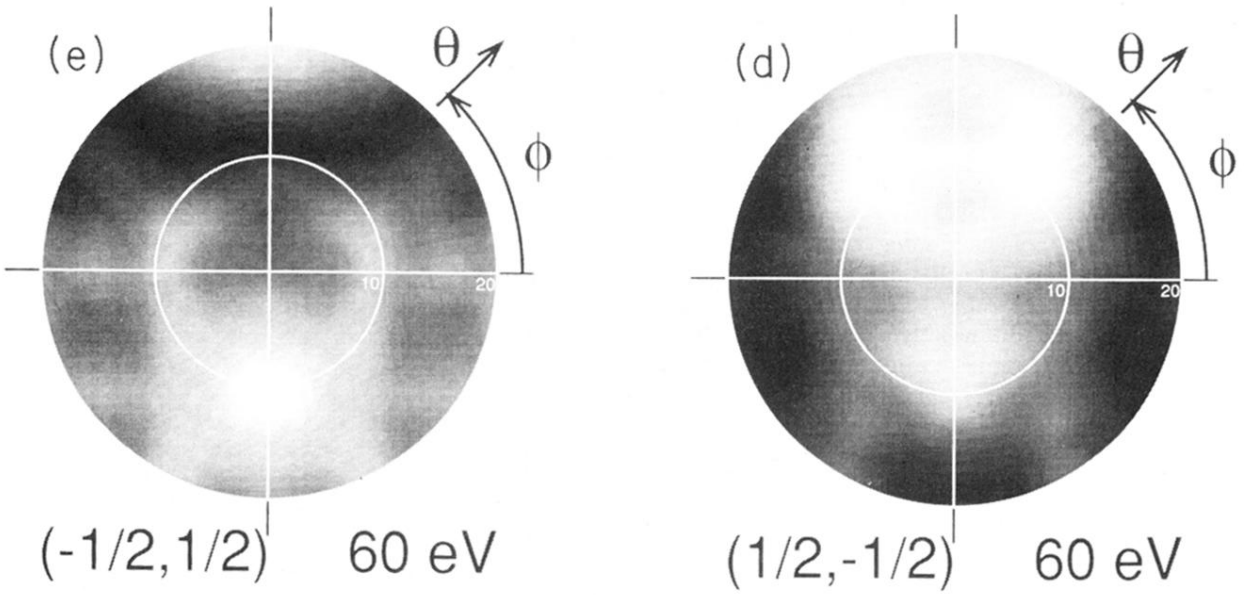

FIG. 2. (*Continued*).